

# Ibn Al-Haitham Journal for Pure and Applied Sciences

Journal homepage: jih.uobaghdad.edu.iq PISSN: 1609-4042, EISSN: 2521-3407 IHJPAS. 2025, 38(4)



# Synthesis and Characterization of a Magnetically Functionalized Silver-Curcumin-Chitosan Nanocomposite using Super Magnetite

Hiba Ali Alzand¹ <sup>™</sup> and Entisar E. Al-Abodi²\* <sup>™</sup>

<sup>1,2</sup>Department of Chemistry, College of Education for Pure Science (Ibn Al-Haitham), University of Baghdad, Baghdad, Iraq.
\*Corresponding Author.

Received: 18 December 2024 Accepted: 23 April 2025 Published: 20 October 2025

doi.org/10.30526/38.4.3656

#### **Abstract**

Green synthesis of nanoparticles (NPs) has gained attention as an eco-friendly alternative to conventional methods, reducing toxicity to the environment and living organisms. This study aims to synthesize a novel nanocomposite (Mag-Chi-Cur-AgNPs) composed of silver NPs (AgNPs) prepared using curcumin (Cur) as a reducing and stabilizing agent, along with chitosan (Chit) and magnetic iron oxide (Mag). Cur-AgNPs were synthesized by dissolving Cur in dimethyl sulfoxide and deionized water, followed by the controlled addition of AgNO<sub>3</sub>. The solution was stirred, pH-adjusted, ultrasonicated, and incubated. Chit-Cur-Ag nanocomposite was formed by dissolving nanochitosan in acetic acid, mixing it with Cur-AgNPs, then stirring, washing, centrifuging, and drying. Finally, Mag-Chit-Cur-AgNPs were obtained by coating Chit-Cur-AgNPs with magnetic iron oxide. Characterization techniques confirmed the formation of the nanocomposite. The ultraviolet-visible spectrum is used to track synthesis stages and successful formation. Fourier transform infrared spectroscopy is used to identify bond peaks, verifying molecular changes, in the field. Emission scanning electron microscope analysis measured the nanocomposite size, with particles below 100 nm. X-ray diffraction is used to determine the crystalline structure and dimensions of each component. Magnetic properties were analyzed using a vibrating sample magnetometer, demonstrating high magnetic saturation. This study successfully synthesized and characterized Mag-Chi-Cur-AgNPs using green chemistry. The results confirmed the formation and stability of the nanocomposite, showcasing its potential for future biomedical and technological applications.

Keywords: Chitosan, Green chemistry, Magnetite, Nanoparticles, Silver-curcumin.

#### 1. Introduction

With the rise of multidrug-resistant microorganisms and increasing healthcare costs, efforts have been made to develop novel, effective, cost-efficient antimicrobial agents with minimal resistance, which offer broad-spectrum efficacy and a lower tendency to induce microbial resistance than antibiotics (1). Consequently, research has shifted towards natural and traditional alternative medicines. Curcumin (*Curcuma longa L.*), commonly known as turmeric, is a widely studied compound from the *Zingiberaceae* family due to its anti-inflammatory, antimicrobial, wound-healing, and skin-lightening properties (2). However, its

poor water solubility at normal pH, rapid metabolism, and low bioavailability limit its direct pharmaceutical application (3). To enhance the therapeutic potential of Cur, research has focused on its chelation with metals or combination with other nutritional agents. Its antimicrobial effect has been attributed to the down-regulation of 5,6-dehydrotase (ERG3) (4). Nanomaterials, defined as materials with at least one dimension between 1 and 100 nm, have received significant attention due to their unique electrical, optical, and mechanical properties (5,6). Their applications in pharmaceuticals and healthcare include drug delivery, tissue engineering, and biosensors. While various chemical and physical methods are used for nanomaterial synthesis, they often involve toxic solvents, hazardous byproducts, and high energy consumption. Therefore, green synthesis methods have become increasingly favored due to their efficiency, cost-effectiveness, and environmental safety. These eco-friendly approaches allow nanoparticles (NPs) to be synthesized with diverse compositions, sizes, and shapes, making them applicable to modern technological fields (7,8). Silver NPs (AgNPs), in particular, have demonstrated broad-spectrum antimicrobial activity. They are low toxicity to mammalian cells but highly toxic to microbial agents through free radical generation and oxidative stress induction (10<sup>-13</sup>). Chitosan (Chit), a polysaccharide derived from chitin, has a molecular weight ranging from 300 to 1000 kDa, depending on its source. It is the second most abundant natural polymer after cellulose, primarily obtained from crustaceans such as crabs and shrimp (9). Chitosan has been widely utilized in biomedical applications, including tissue engineering, wound healing, gene delivery, and various drug delivery systems (10,11). Magnetic nanostructures have a high surface area-to-volume ratio and ease of surface modification (12, 13). Their movement can be controlled using an external magnetic field (14). For biomedical applications, biocompatibility and toxicity are critical factors influenced by the magnetically responsive component's composition (15). This study aims to synthesize Mag-Chit-Cur-AgNPs by incorporating green AgNPs and Chit onto iron oxide (Fe<sub>3</sub>O<sub>4</sub>) nanomaterials, enhancing the properties of the Mag-Chit-Cur-AgNPs composite. This modification increases the electron pair lifetime and the energy gap between components, making the composite highly promising for various applications.

#### 2. Materials and Methods

All chemicals used in this article were obtained from Sigma Aldrich and used without purification.

### 2.1. Preparation of Cur-AgNPs

Curcumin extract was prepared following a previously reported method (16); Cur (0.07368 g) was dissolved in 5 mL of dimethyl sulfoxide until fully dissolved, followed by the addition of 10 mL of deionized water. A 5 mL aqueous solution of silver nitrate (AgNO<sub>3</sub>, 0.1 M) was then mixed at 50°C for 30 min, with the flask covered in aluminum foil to prevent light-induced reactions. Subsequently, the Cur solution was gradually added dropwise under continuous magnetic stirring for 15 min. If necessary, the pH was adjusted to 7–9 by adding 1% NaOH solution until a color change from yellow to brownish was observed. Stirring was continued for 30 min, followed by ultrasonication for 30 min, and incubation in a shaking incubator for 24 hours (17).

### 2.2. Preparation of Cur-Ag-Chit

Nanochitosan (0.3 g) was dissolved in 20 mL of 1% acetic acid and mixed for 2 hours at room temperature. Meanwhile, 60 mL of the prepared Cur-AgNPs solution was placed in a 100 mL flask and stirred for 1 hour. The nanochitosan solution was gradually added to the mixture while stirring. After the addition, stirring continued for 30 min, and the solution was left

undisturbed for 4–6 hours. The prepared solution was washed 3–4 times with deionized water, centrifuged at 9000 rpm for 15 min, and then dried in an oven at 50°C.

### 2.3. Preparation of Mag-Chit-Cur-AgNPs nanocomposite

Magnetic NPs were coated with Chit-Cur-AgNPs to synthesize Mag-Chit-Cur-AgNPs using the self-assembly method. Magnetite NPs, synthesized via co-precipitation of Fe<sup>3+</sup> and Fe<sup>2+</sup> ions in an alkaline medium, were added to the Chit-Cur-Ag nanocomposite (18). To collect the final nanocomposite, the solution was centrifuged at 4000 rpm for 5 min, dried, and characterized using ultraviolet-visible (UV-vis), Fourier transform infrared spectroscopy (FTIR), and field emission scanning electron microscopy (FESEM) analysis, as shown in **Figure 1**.

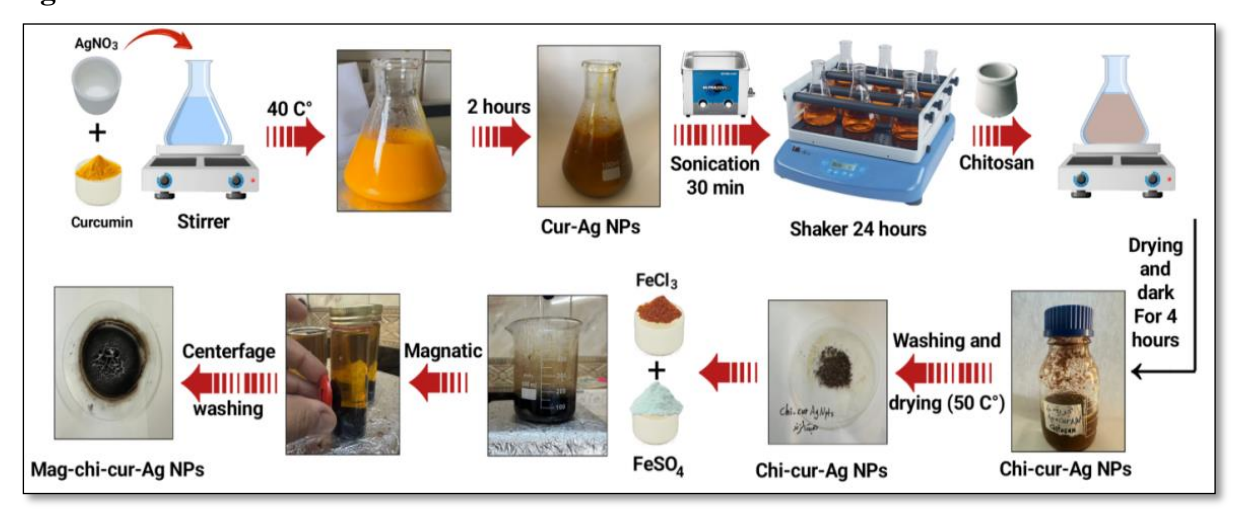


Figure 1. The methodology for preparation of Mag-Chit-Cur-AgNPs nanocomposite.

#### 3. Results

### 3.1. The UV-visible spectra

**Figure 2** presents the UV-Vis analysis of the prepared nanocomposite. The absorption peaks of the added materials for the formation of the nanocomposite.

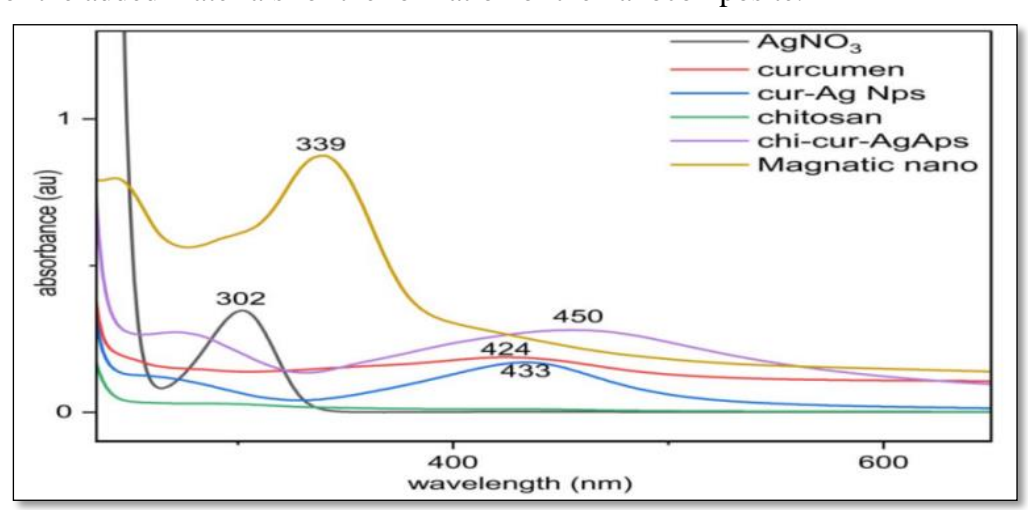
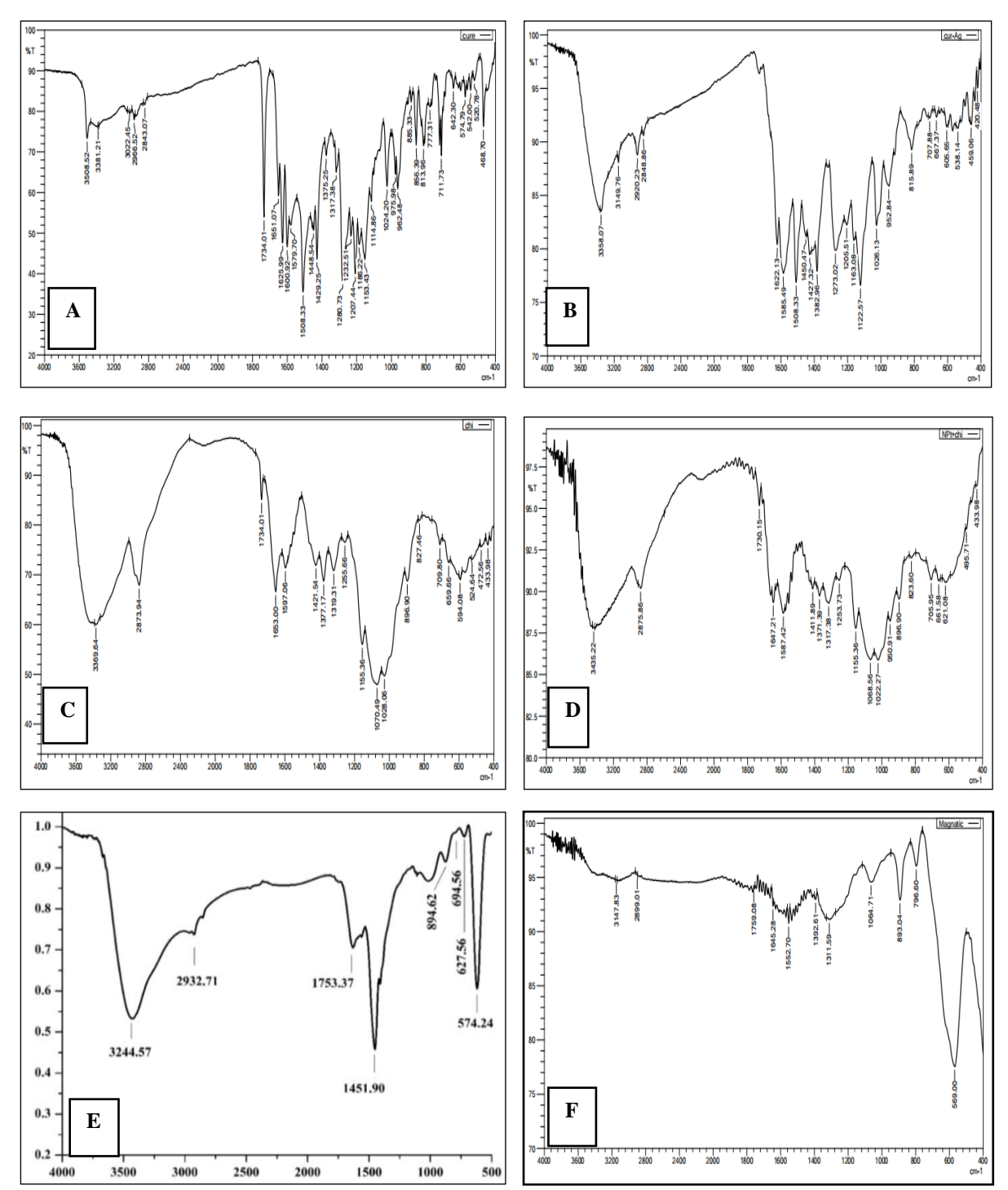


Figure 2. The UV-vis spectrum of samples.

## 3.2. The FTIR spectra

The FTIR spectra of Cur, Cur-AgNPs, Chit, Chit-Cur-AgNPs, and Mag-Chit-Cur-AgNPs (**Figure 3**) were recorded using a SHIMADZU FTIR spectrometer.



 $\textbf{Figure 3.} \ \, \textbf{The FTIR analysis of (A)} \ \, \textbf{Cur (B) Cur-AgNPs (C) chitasan (D) Chit-Cur-AgNPs (E) Fe}_{3}O_{4} \, (\textbf{F) Mag-Chit-Cur-AgNPs}. \\$ 

### 3.3. The FESEM

The FESEM is a high-resolution technique used for nanoscale material characterization. It scans the sample surface with a focused beam of activated electrons, providing information about texture, crystal structure, and chemical composition, as shown in **Figure 4**.

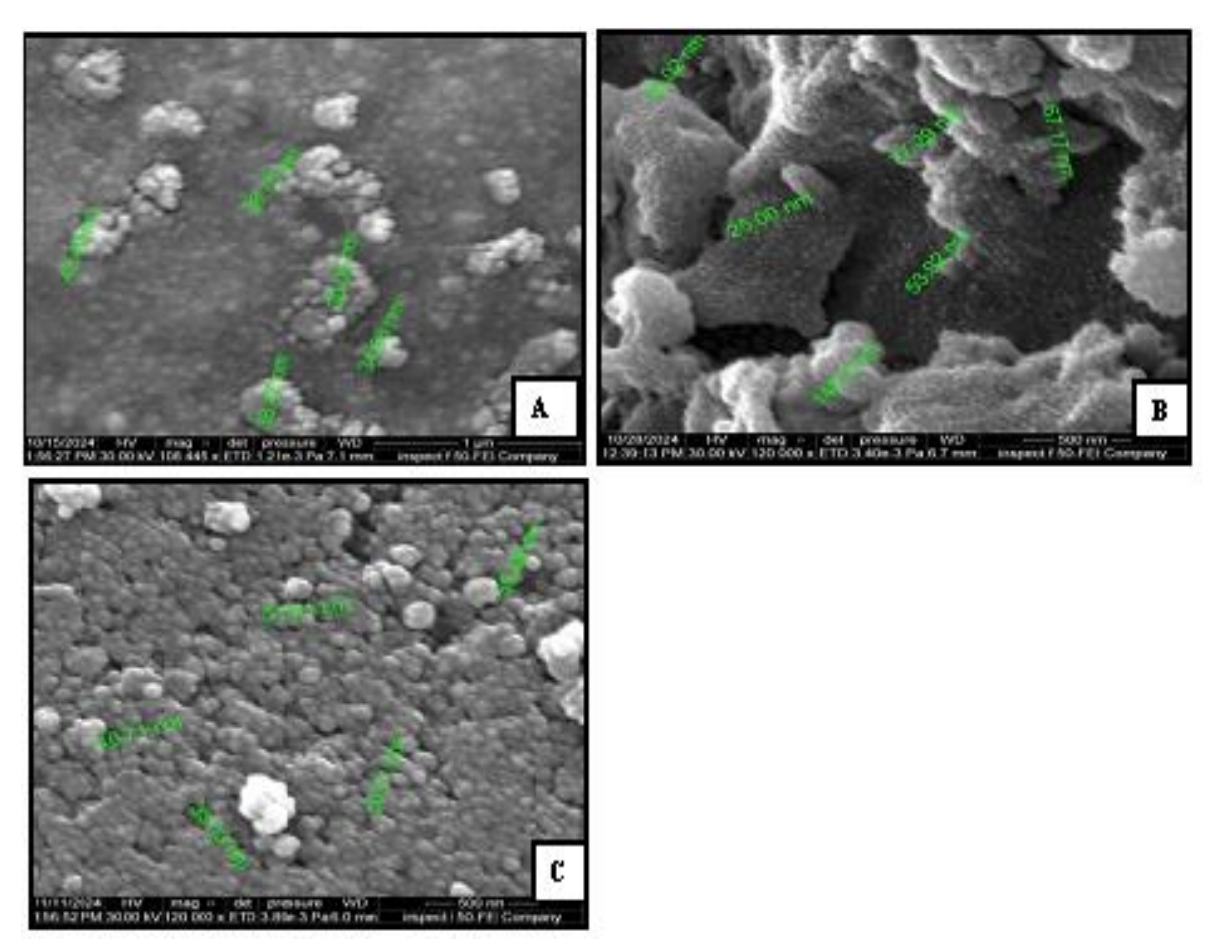


Figure 4. The FESEM (A) CurAgNPs (B) Chit-CurAgNPs (C) Mag-Chit-CurAg NPs.

# 3.4. X-ray diffraction

The X-ray diffraction (XRD) of the specimens was obtained using a Bruker D8 Advance X-ray diffractometer with  $CuK\alpha$  radiation and  $2\theta/\theta$  scanning mode. Data collected over a  $2\theta$  range of  $30–80^\circ$ , the average crystallite size (D) was determined using the Debye-Scherrer formula (19), as shown in **Figure 5**. The XRD data for the analyzed samples are summarized in **Table 1**, representing the information from the Matched by (References code) from the analyses.

**Table 1.** The XRD data of samples.

| Formula           | Matched by (References code) | Element           | Crystal system | <b>A</b><br>(Å) | B<br>(Å) | C<br>(Å) | Mean<br>particle size |
|-------------------|------------------------------|-------------------|----------------|-----------------|----------|----------|-----------------------|
| AgNO <sub>3</sub> | 01-070-0779                  | AgNO <sub>3</sub> | Orthorhombic   | 10.125          | 7.335    | 6.992    | 82.660                |
| Cur-<br>AgNPs     | 01-087-0719                  | Ag                | Cubic          | 4.071           | 4.071    | 4.071    | 43.297                |
| Chit              | 01-074-2330                  | carbon            | Orthorhombic   | 2.460           | 4.260    | 28.960   | 26.484                |
| Chit-Cur-         | 01-087-0597                  | Ag                | Cubic          | 4.086           | 4.086    | 4.086    | 16.101                |
| AgNPs             | 00-026-1077                  | Carbon            | Hexagonal      | 2.456           | 2.456    | 16.740   |                       |
| $Fe_3O_4$         | 00-039-1346                  | Iron              | Cubic          | 8.351           | 8.351    | 8.351    | 37.554                |
| Mag-Chit-         | 01-087-0719                  | Ag                | Cubic          | 4.071           | 4.071    | 4.071    |                       |
| Cur-              | 01-074-2330                  | Carbon            | Orthorhombic   | 2.460           | 4.260    | 28.960   | 44.424                |
| AgNPs             | 01-087-0722                  | Iron              | Cubic          | 2.860           | 2.860    | 2.860    |                       |

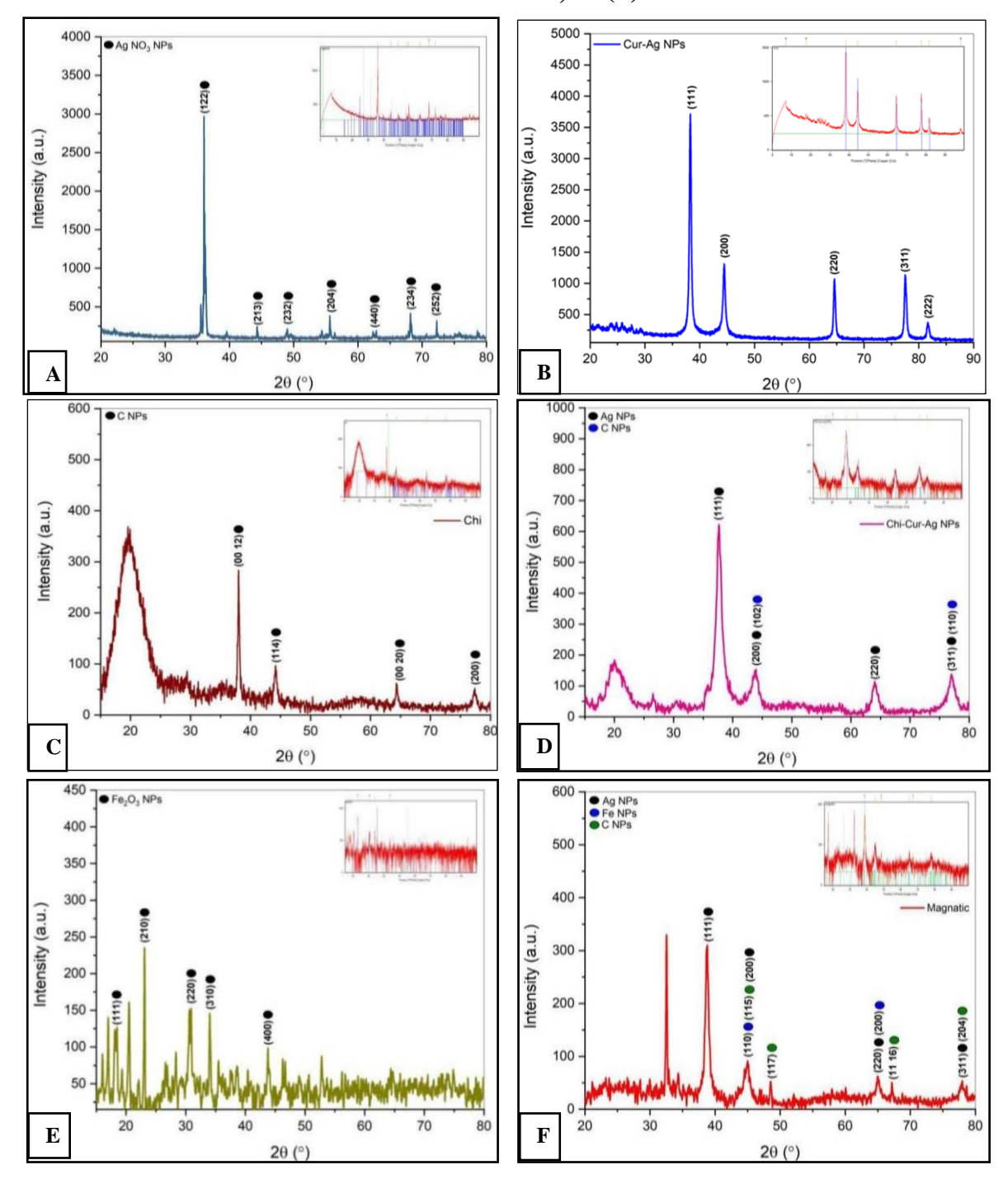
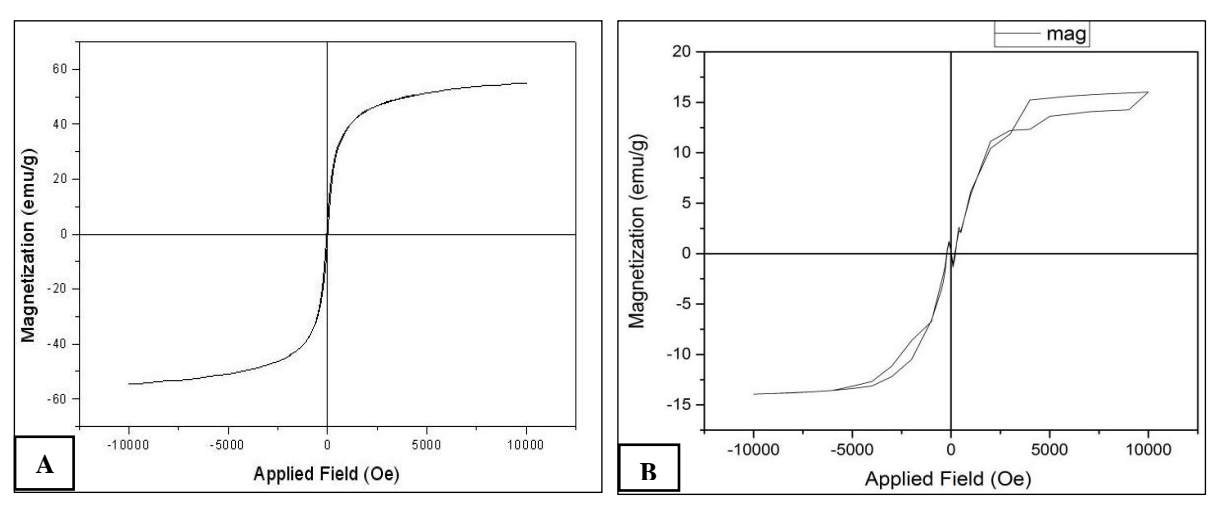


Figure 5. The XRD of (a)  $AgNO_3$  (b) Cur-AgNPs (c) Chit (d) Chit-Cur-AgNPs (e)  $Fe_3O_4$  (f) Mag-Chit-Cur-AgNPs.

# 3.5. The vibrating sample magnetometer

The magnetic properties of the nanocomposite prepared from AgNPs, Cur, and Chit, after magnetization by adding iron, were measured using a vibrating sample magnetometer (VSM), as illustrated in **Figure 6**.



**Figure 6.** The VSM of (a) Fe<sub>3</sub>O<sub>4</sub> (b) (Mag) Fe<sub>3</sub>O<sub>4</sub>-Chit-Cur-AgNPs.

#### 4.Discussion

#### 4.1. Characterization

# 4.1.1. The UV-vis spectra

**Figure 2** presents the UV-vis analysis as follows: the AgNO<sub>3</sub> solution, no clear peak was observed in the visible region (400–700 nm), although a peak at 302 nm, attributed to silver ions (Ag<sup>+</sup>), was detected, as previously reported in the literature (20). A prominent peak at 433 nm was observed, corresponding to the localized surface plasmon resonance (LSPR) absorption of AgNPs, indicating a red shift compared to Cur alone (424 nm) due to increased absorbance. The absorption peak shifted further to 450 nm after adding Chit, suggesting an increase in the nanocomposite size. Mag-Chit-Cur-AgNPs resulted in an absorption peak at 339 nm, consistent with previous reports, where magnetization caused a blue shift, indicating a reduction in particle size. After nanoparticle formation, changes in absorption bands were observed.

### 4.1.2. The FTIR spectra

Comparing Cur and Cur-AgNP in Figure 3A and 3B, the peaks at 3358.07 cm<sup>-1</sup> (phenolic OH stretching) and 2920.23 cm<sup>-1</sup> (asymmetric C-H stretching of -OCH<sub>3</sub> groups) appear in both spectra, indicating that phenolic hydroxyl and methoxy groups are not involved in the reduction process (21). Peaks at 1508.33 cm<sup>-1</sup>, 1026.13 cm<sup>-1</sup>, and 952.84 cm<sup>-1</sup> in Cur-AgNP correspond to aliphatic C-H stretches and aromatic C-C-C and C-CH vibrations. The C=C and C=O stretching peak at 1625.99 cm<sup>-1</sup> in Cur shifts to 1622.13 cm<sup>-1</sup> in Cur-AgNP. Additionally, the disappearance of 1153.43 cm<sup>-1</sup> and 1280.73 cm<sup>-1</sup> (enol C-O absorption) and the emergence of a peak at 1375 cm<sup>-1</sup> confirm silver association with the C=O group, indicating Cur coating and functionalization (22). The FTIR of Chit-NPs in Figure 3C shows strong absorption at 3369.64 cm<sup>-1</sup> (symmetric OH and NH stretching) and 2873.94 cm<sup>-1</sup> (-CH<sub>2</sub> in pyranose ring) (23). Peaks at 1663 cm<sup>-1</sup> and 1557.06 cm<sup>-1</sup> correspond to amide C=O stretching and NH bending, while 1421 cm<sup>-1</sup> and 1377 cm<sup>-1</sup> are attributed to CH<sub>3</sub> amide. Peaks at 1255.99 cm<sup>-1</sup> and 1319 cm<sup>-1</sup> indicate C-N stretching, with a broad band at 1070.49 cm<sup>-1</sup> representing C-O stretching in Chit (24). For Chit-Cur-Ag in Figure 3D characteristic Chit bands appear at 3369.64 cm<sup>-1</sup>, 2917 cm<sup>-1</sup>, and 1426 cm<sup>-1</sup>, shifted from 3435.22 cm<sup>-1</sup>, 2875.86 cm<sup>-1</sup>, and 1411 cm<sup>-1</sup>, indicating interaction with AgNPs. The 1663 cm<sup>-1</sup> band shifts to 1647.21 cm<sup>-1</sup>, representing NH bending, while 1070.49 cm<sup>-1</sup> signifies overlapping alcoholic C-O and ether-stretching bands (25, 26).

The FTIR spectrum of Mag-NPs in **Figure 3E** confirms Fe<sub>3</sub>O<sub>4</sub> presence with Fe–O stretching vibrations at 627.56 cm<sup>-1</sup> and 574.24 cm<sup>-1</sup>. Peaks at 3244.57 cm<sup>-1</sup> and 2932.71 cm<sup>-1</sup>

correspond to O-H stretching from adsorbed moisture, with additional Fe–O peaks at 607.58 cm<sup>-1</sup> and 717.32 cm<sup>-1</sup>. Peaks at 1620.21 cm<sup>-1</sup> and 3377.36 cm<sup>-1</sup> indicate O-H bending and stretching, respectively (27, 28). The FTIR of Mag-Chit-Cur-AgNPs in **Figure 3F** retains characteristic bands from Chit-Cur-AgNPs and Fe<sub>3</sub>O<sub>4</sub>, with a strong Fe–O absorption peak at 569 cm<sup>-1</sup>. Additional bands at 3147.03, 2899.01, 1552.7, 1311.59, 1064.71, 893.04, and 796.60 cm<sup>-1</sup> suggest chemisorption of Chit-Cur-AgNPs onto magnetite (28, 29).

#### **4.1.3. The FESEM**

In **Figure 4A**, FESEM analysis of the Cur-AgNPs sample revealed nanoparticle sizes ranging from 25 to 45 nm, as indicated by the green color. The morphology appeared as small, adjacent, and stacked spherical structures with randomly distributed light and dark areas (29). In **Figure 4B**, the FESEM analysis of the Chit-Cur-AgNPs showed an increase in particle size (25–150 nm) as a green indicator due to adding Chit, a polymeric material. The morphology exhibited more adhesions, reduced sphericity, and a structure resembling a cut cauliflower. In **Figure 4C**, after the addition of Fe<sub>3</sub>O<sub>4</sub>, the average nanoparticle size of Mag-Chit-Cur-AgNPs decreased to 40–60 nm, and the morphology became more spherical. The presence of iron contributed to a clear and consistent spherical structure, with adjacent packed NPs and visible gaps. Additionally, light-colored spheres observed in the image were attributed to Chit (30).

#### 4.1.4. The XRD

The XRD spectrum of Cur exhibited strong diffraction peaks at  $2\theta$ = 8.9°, 14.5°, 17.26°, 18°, 21.05°, 23.5°, 24.6°, and 28.2°, indicating its crystalline nature. **Figure 5A** was compared with the JCPDS standard card No. 01-070-0779 in the XRD pattern of silver metal, four main peaks at  $2\theta$ = 38.2901°, 44.5583°, 64.8185°, 68.55°, and 78°, corresponding to the (hkl) values (122), (213), (440), (234), and (311), confirmed the presence of Ag nanostructures with a face-centered cubic crystal structure. The average crystallite size of Ag NPs was 20 nm (30,31).

The XRD pattern of Chit composite in **Figure 5B** displayed characteristic peaks at  $2\theta$ = 29.3398°, 34.0575°, 17.9885°, 37.8823°, 44°, 64°, and 22.9512°, consistent with JCPDS card No. 39-1894. The peaks at  $2\theta$ = 11.7° and 20.2° aligned well with literature values (32). The broadening of peaks indicated the amorphous nature of Chit. In **Figure 5D**, the XRD pattern of the Chit-Cur-AgNPs showed peaks corresponding to both chitosan and Cur-AgNPs. Chit peaks were observed at  $2\theta$ = 11.7° and 19.8°, while silver peaks were found at 37.9°, 44.0°, and 63.9° (33). The XRD pattern of magnetite NPs (Mag NPs) in **Figure 5E** confirmed the highly crystalline structure of Fe<sub>3</sub>O<sub>4</sub>. Characteristic peaks at  $2\theta$ = 19°, 23°, 31°, 34°, and 44°, corresponding to the (hkl) values= 111, 210, 220, 310, and 400, confirmed the spinel crystal structure of magnetite Fe<sub>3</sub>O<sub>4</sub>, in agreement with previous studies (34). The XRD of the (Mag-Chit-CurAg NPs) **Figure 5F** exhibited sharp peaks at  $2\theta$ = 38°, 44°, 45°, 48°, 65°, 67°, and 77° (Ag), along with distinct peaks at 45° and 65° for Fe<sub>3</sub>O<sub>4</sub>. A broad peak at  $2\theta$ = 22°, 37°, 45°, and 48° corresponded to Chit. The presence of these peaks without significant overlap or distortion confirmed the successful formation of the nanocomposite. The XRD results verified that Ag and Fe<sub>3</sub>O<sub>4</sub> retained their crystalline nature, while Chit provided an amorphous matrix.

### 4.1.5. The VSM characterization

The curve shows the nanocomposite exhibits a remnant magnetization of approximately  $\pm 7$  emu/g at zero field, indicating that the material retains magnetic properties after removing the external field. The saturation magnetization reached 15-20 emu/g, reflecting the presence of a magnetic component in the composite resulting from incorporating iron into the nanocomposite system. Additionally, the coercive field showed a value of approximately

 $\pm 350$  Oe, indicating that the composite requires a specific applied magnetic field to eliminate the remanent magnetization, enhancing the nanocomposite's ability to be directed and controlled by an external magnetic field. These properties make the nanocomposite suitable for biomedical applications, such as directing drugs to specific sites in the body using a magnetic field, thus improving the targeting of affected cells and reducing the side effects of the therapy (35).

When comparing in **Figure 6A**, a higher magnetic saturation of about 60 emu/g is observed, with an apparent magnetic hysteresis and noticeable remanence and coercivity. Curve indicates a material with strong magnetization, such as a material with high iron content, pure  $Fe_3O_4$ .

The graph in **Figure 6B** shows the hysteresis loop, representing the relationship between magnetization and the applied magnetic field.

#### 5. Conclusion

Using green chemistry principles, this study synthesized a novel nanocomposite (Mag-Chit-CurAg NPs). The nanocomposite was formulated with precisely calculated amounts of AgNPs, which were biosynthesized using Cur as a natural reducing and stabilizing agent. Additionally, Chit was incorporated as a biopolymeric matrix, while magnetic Fe<sub>3</sub>O<sub>4</sub>-NPs were included to impart magnetic properties. The structural and physicochemical characteristics of the synthesized nanocomposite were comprehensively analyzed using various characterization techniques, confirming the successful formation of the designed material. The biological significance of this nanocomposite lies in its multifunctional properties. Cur and AgNPs are well known for their potent antimicrobial, antioxidant, and anti-inflammatory effects, while Chit enhances biocompatibility and stability. Magnetic Fe<sub>3</sub>O<sub>4</sub> enables potential applications in targeted drug delivery and biomedical imaging.

#### Acknowledgment

The authors thank the Department of Chemistry/ College of Education for Pure Science (Ibn Al-Haitham)/ University of Baghdad for providing chemicals and support.

#### **Conflict of Interest**

The authors declare that they have no conflicts of interest.

### **Funding**

No funding.

#### **Ethical Clearance**

The Scientific Committee at the Department of Chemistry, College of Education for Pure Science (Ibn Al-Haitham), University of Baghdad, has approved this work, No. 680, on 17/9/2024.

#### References

- 1. Jones DL, Hodge A, Kuzyakov Y. Plant and mycorrhizal regulation of rhizodeposition. New Phytol. 2004; 163(3):459–480. https://doi.org/10.1111/j.1469-8137.2004.01130.x.
- Yang F, Lim GP, Begum AN, Ubeda OJ, Simmons MR, Ambegaokar SS, Chen PP, Kayed R, Glabe CG, Frautschy SA, Cole GM. Curcumin inhibits formation of amyloid β oligomers and fibrils, binds plaques, and reduces amyloid in vivo. J Biol Chem. 2005; 280(7):5892–5901. <a href="https://doi.org/10.1074/jbc.M404751200.">https://doi.org/10.1074/jbc.M404751200.</a>

- 3. Karthikeyan A, Senthil N, Min T. Nanocurcumin: A promising candidate for therapeutic applications. Front Pharmacol. 2020; 11:487. https://doi.org/10.3389/fphar.2020.00487.
- 4. Alavi M, Rai M, Shende S, Abd-Elsalam KA, Bajpai VK. Nanoformulations of curcumin and quercetin with silver nanoparticles for inactivation of bacteria. Cell Mol Biol. 2021; 67(5):151–156. http://dx.doi.org/10.14715/cmb/2021.67.5.21.
- 5. Bamal D, Singh A, Chaudhary G, Kumar M, Singh M, Rani N, Mundlia P, Sehrawat AR. Silver nanoparticles biosynthesis, characterization, antimicrobial activities, applications, cytotoxicity and safety issues: An updated review. Nanomaterials. 2021; 11(8):2086. https://doi.org/10.3390/nano11082086.
- 6. Atiya MA, Hassan AK, Kadhim FQ. Green synthesis of copper nanoparticles using tea leaves extract to remove ciprofloxacin (CIP) from aqueous media. Iraqi J Sci. 2021; 62(9):2832–2854. https://doi.org/10.24996/ijs.2021.62.9.1.
- 7. Jdayea NA, Al-Abodi EE. Biosynthesis of nanoparticles from plant extracts and their applications in medical treatments and drug delivery. Anbar J Agric Sci. 2024; 22(2):1240–1259. https://doi.org/10.32649/ajas.2024.184478.
- 8. Naif TA, Ahmed BJ. Synthesis, characterization and study of the effect of nanoparticles on the biological activity of new silicon polymers and their nanocomposites. Iraqi J Phys Appl Sci. 2024; 37(4): 312–322. https://doi.org/10.30526/37.4.3391.
- 9. Mishra B, Yadav AS, Malhotra D, Mitra T, Sinsinwar S, Radharani NNV, Rajendran M, Dey A, Shukla R. Chitosan nanoparticle-mediated delivery of curcumin suppresses tumor growth in breast cancer. Nanomaterials. 2024; 14(15):1294. https://doi.org/10.3390/nano14151294.
- 10.Wu Y, Zhang R, Tran HD, Kurniawan ND, Moonshi SS, Whittaker AK, Ghosh D, Nisbet DR. Chitosan nanococktails containing both ceria and superparamagnetic iron oxide nanoparticles for reactive oxygen species-related theranostics. ACS Appl Nano Mater. 2021;4(4):3604–3618. https://doi.org/10.1021/acsanm.1c00141.
- 11.Zaki NH, AlKaram LK, Alnuaimi M. Introduction to nanotechnology world. 1<sup>st</sup> ed. Baghdad: Adnan Library; 2024.
- 12. Christian P, Von der Kammer F, Baalousha M, Hofmann T. Nanoparticles: structure, properties, preparation and behaviour in environmental media. Ecotoxicology. 2008; 17(5):326–343. <a href="https://doi.org/10.1007/s10646-008-0213-1">https://doi.org/10.1007/s10646-008-0213-1</a>.
- 13. Ahmed OA, Abed AH, Al-Saadi TM. Magnetic properties and structural analysis of Ce-doped Mg—Cr nano-ferrites synthesized using auto-combustion technique. Macromol Symp. 2022; 401(1):2100311. https://doi.org/10.1002/masy.202100311.
- 14.Majeed AR, Al-Robaie AE. Majeed AA, Al-Robaie EA. Study the effect of adding citric acid as a fuel on the structural characteristics of the nano spinel ferrite (NiO.1CuO.2Zn0.7Fe<sub>2</sub>O<sub>4</sub>) synthesized by sol–gel auto combustion method. IHJPAS. 2015; 28(3):399-409.
- 15. Nowak-Jary J, Machnicka B. Comprehensive analysis of the potential toxicity of magnetic iron oxide nanoparticles for medical applications: Cellular mechanisms and systemic effects. Int J Mol Sci. 2024; 25(22):12013. <a href="https://doi.org/10.3390/ijms252212013">https://doi.org/10.3390/ijms252212013</a>.
- 16.Mohankumar S, McFarlane JR. An aqueous extract of *Curcuma longa* (turmeric) rhizomes stimulates insulin release and mimics insulin action on tissues involved in glucose homeostasis *in vitro*. Phytother Res. 2011; 25(3):396–401. https://doi.org/10.1002/ptr.3275.
- 17. Jaiswal S, Mishra P. Antimicrobial and antibiofilm activity of curcumin-silver nanoparticles with improved stability and selective toxicity to bacteria over mammalian cells. Med Microbiol Immunol. 2018; 207(1):39–53. https://doi.org/10.1007/s00430-017-0525-y.
- 18.Sadiq YM, Al-Abodi EE. Preparation and characterization of a new nano mixture, and its application as photocatalysis in self-assembly method for water treatment. AIP Conf Proc. 2019; 2190(1):032089. https://doi.org/10.1063/1.5138528.
- 19. Yusuf SI, Mohammad SJ, Ali MH. Scherrer and Williamson-Hall estimated particle size using XRD analysis for cast aluminum alloys. J Theor Appl Phys. 2024; Special Issue AICIS'23:17. <a href="https://doi.org/10.57647/j.jtap.2024.si-AICIS23.17">https://doi.org/10.57647/j.jtap.2024.si-AICIS23.17</a>.

- 20.Luu AT, Nguyen MT, Ta DN, Huynh CD. Fabrication and study on the structural and photocatalytic characterization of Ag doped ZnO nanostructure materials. VNUHCM J Eng Technol. 2023; 6(SI3): 80–87. https://doi.org/10.32508/stdjet.v6iSI3.1262.
- 21.Stati G, Rossi F, Trakoolwilaiwan T, Tung LD, Mourdikoudis S, Thanh NTK, Salvati A, Åberg C, Dawson KA. Development and characterization of curcumin-silver nanoparticles as a promising formulation to test on human pterygium-derived keratinocytes. Molecules. 2022; 27(1):282. <a href="https://doi.org/10.3390/molecules27010282">https://doi.org/10.3390/molecules27010282</a>.
- 22. Sindhu K, Rajaram A, Sreeram KJ, Rajaram R. Curcumin conjugated gold nanoparticle synthesis and its biocompatibility. RSC Adv. 2014; 4(4):1808–1818. <a href="https://doi.org/10.1039/C3RA45345F">https://doi.org/10.1039/C3RA45345F</a>.
- 23.Nasrin Farsana N, Sheik Muhideen Badhusha M, Shakina J, Mohamed Roshan M. Synthesis, structural and anti-microbial application of iron oxide/chitosan/curcumin coated nanoparticles. Eur Chem Bull. 2023; 12(SI4):11371–11383. https://doi.org/10.48047/ecb/2023.12.si4.1026.
- 24.Mumtaz S, Ali S, Mumtaz S, Mughal TA, Tahir HM, Shakir HA. Chitosan conjugated silver nanoparticles: the versatile antibacterial agents. Polym Bull. 2022. <a href="https://doi.org/10.1007/s00289-022-04321-z">https://doi.org/10.1007/s00289-022-04321-z</a>.
- 25. Sanmugam A, Sellappan LK, Sridharan A, Manoharan S, Sairam AB, Almansour AI, Arumugam N, Karuppusamy I. Chitosan-integrated curcumin–graphene oxide/copper oxide hybrid nanocomposites for antibacterial and cytotoxicity applications. Antibiotics. 2024; 13(7):620. <a href="https://doi.org/10.3390/antibiotics13070620">https://doi.org/10.3390/antibiotics13070620</a>.
- 26. Taher NG, Al-Abodi EE. Anticancer activity of synthesized green silver nanoparticles against human colon cancer cell lines. Onkol Radioter. 2023; 17(11):950–960.
- 27.Bordbar AK, Rastegari AA, Amiri R, Ranjbakhsh E, Abbasi M, Khosropour AR. Characterization of modified magnetite nanoparticles for albumin immobilization. Biotechnol Res Int. 2014; 2014:705068. https://doi.org/10.1155/2014/705068.
- 28. Hartati H, Subaer S, Hasri H, Wibawa T, Hasriana H. Microstructure and antibacterial properties of chitosan-Fe<sub>3</sub>O4-AgNP nanocomposite. Nanomaterials. 2022; 12(20):3652. https://doi.org/10.3390/nano12203652.
- 29.Ali MN, Al-Saadi TM, Al-Faragi JK. Effect of chitosan nanoparticles loaded oxytetracycline hydrochloride on health status of common carp (Cyprinus carpio L.) infected with columnaris disease. J Phys Conf Ser. 2021; 1879(3):032075. <a href="https://doi.org/10.1088/1742-6596/1879/3/032075">https://doi.org/10.1088/1742-6596/1879/3/032075</a>.
- 30.Abd El-Hady MM, El-Sayed Saeed S. Antibacterial properties and pH sensitive swelling of in situ formed silver–curcumin nanocomposite based chitosan hydrogel. Polymers. 2020; 12(11):2451. <a href="https://doi.org/10.3390/polym12112451">https://doi.org/10.3390/polym12112451</a>.
- 31.Al-Saadi TM, Alsaady LJ. Preparation of silver nanoparticles by sol-gel method and study their characteristics. IHJPAS. 2015; 28(1):301–310.
- 32. Saleem MH, Ahmed BJ. Synthesis, characterization and study bioactivity of silver nanocomposites. Int J Pharm Res. 2020; 12(4):766–772. https://doi.org/10.31838/ijpr/134.
- 33. Abduljabar MA, Merza SH. Synthesis, characterization of nickel cobaltite nanoparticles and its use in removal methyl green dye from aqueous solution. IHJPAS. 2024; 37(3):264–276. https://doi.org/10.30526/37.3.3398.
- 34.Tran BLT, Vo TV, Chu TP, Bach DT, Nguyen TQ, Luu PHB, Nguyen TT, Nguyen TH, Le TT, Nguyen HQ. Antibacterial efficacy of low-dosage silver nanoparticle–sodium alginate–chitosan nanocomposite films against pure and clinical acne strains. RSC Adv. 2024; 14(45):33267–33280. https://doi.org/10.1039/d4ra05180g.
- 35. Shareef AA, Hassan ZA, Kadhim MA, Al-Mussawi AA. Antibacterial activity of silver nanoparticles synthesized by aqueous extract of Carthamus oxycantha M. Bieb. against antibiotics resistant bacteria. Baghdad Sci J. 2022; 19(3):460–470. <a href="http://dx.doi.org/10.21123/bsj.2022.19.3.0460">http://dx.doi.org/10.21123/bsj.2022.19.3.0460</a>.